JOURNAL OF EXPERIMENTAL AND THEORETICAL PHYSICS, 2024, VOL. 165, No. 1, pp. 1–7

## ATOMS, MOLECULES, OPTICS

# DETERMINATION OF THE BINDING ENERGY AND STRUCTURE OF VAN DER WAALS COMPLEXES OF OXYGEN WITH XENON $Xe_n - O_2(n = 1,2)$

© 2024 V. M. Rogoveshko[a, b*], A. S. Bogomolova, A. V. Baklanova

[a]Voevodsky Institute of Chemical Kinetics and Combustion, 630090, Novosibirsk, Russia

[b]Novosibirsk State University, 630090, Novosibirsk, Russia

*e-mail: v.rogoveshko@g.nsu.ru

Received 02.05.2023
Revised 02.05.2023
Accepted 20.05.2023

**Abstract**. Interest in van der Waals complexes of oxygen with xenon is due to the alleged participation of such complexes in providing anesthetic action of xenon in medicine The work is devoted to the measurement of the intermolecular binding energy in van der Waals complexes of oxygen with xenon in $Xe_n$-$O_2$. Van der Waals complexes of oxygen with xenon were generated in a pulsed molecular beam. The velocity map imaging technique was used to measure the energy distribution and the angular distribution anisotropy over the recoil directions of oxygen atoms arising in the photodissociation of these complexes in the $Xe_n$-$O_2$+hν→ $Xe_n$+O+O process. The angular distribution over the recoil directions of oxygen atoms with respect to the direction of the polarization of the exciting radiation indicates the dominant contribution of T-shaped complexes, in which xenon atoms are oriented perpendicular to the axis of the $O_2$ molecule. At a low xenon content in the expanding gas mixture, the dominant contribution is provided by T-shaped Xe-$O_2$ complexes with van der Waals binding energy of 156 ± 11 $cm^{-1}$. With an increase in the xenon concentration, the T-shaped complexes with higher binding energy appear. It is concluded that these complexes have structure $Xe_2$-$O_2$. This assignment is confirmed by the measured velocity map of $Xe^+$ ions which indicates the presence of dimers $Xe_2$ in molecular beam at these conditions. The energy of the van der Waals binding of $O_2$ with $Xe_2$ in $Xe_2$-$O_2$ complex was determined to be 314 ± 30 $cm^{-1}$, and the structure of these complexes was also proposed.

**Keywords**: molecular beams, van der Waals complexes, xenon, oxygen, velocity map imaging technique

**DOI:** 10.31857/S00444510240104e8

## 1. INTRODUCTION

The van der Waals complexes of xenon with oxygen are of interest due to the anesthetic action of xenon discovered in the middle of the last century [1]. Xenon is used in modern anesthesia because its use does not lead to side effects, but so far this action of xenon has not been explained. It should be noted that xenon is a noble gas, which allows us to exclude a chemical mechanism of xenon action. Several hypotheses have been proposed in the literature to explain the anesthetic effect of xenon by the formation of van der Waals complexes with it [2–5]. The authors of [4] found a difference in the anesthetic effect of different xenon isotopes, which was explained by the influence of the nuclear spin of xenon atoms on the radical pairs recombination. To explain this effect, the mechanism of xenon action was proposed in [5], which includes the participation of van der Waals complexes of oxygen with xenon. Thereby, it is important to study the structure and binding energy in such complexes.

Several works [6–8] have been devoted to the study of the structure and binding energy in the simplest xenon-oxygen complexes Xe-$O_2$. Aquilanti et al. studied oxygen molecules scattering on Xe atoms in molecular beams [6]. As a result of these measurements, the authors concluded that the most stable configuration of the Xe-$O_2$ complex is a T-shaped complex in which the xenon atom is located opposite the center of mass of the $O_2$ molecule at a distance of 3.87 Å. The obtained van der Waals binding energy in this complex was 144 $cm^{-1}$ [6]. In the same work, Aquilanti et al. also determined the potential parameters of a less stable linear complex of Xe-$O_2$. Wu et al. determined the equilibrium geometry of the Xe-$O_2$ complex by measuring the kinetic energy of photoions resulting from the Coulomb explosion of

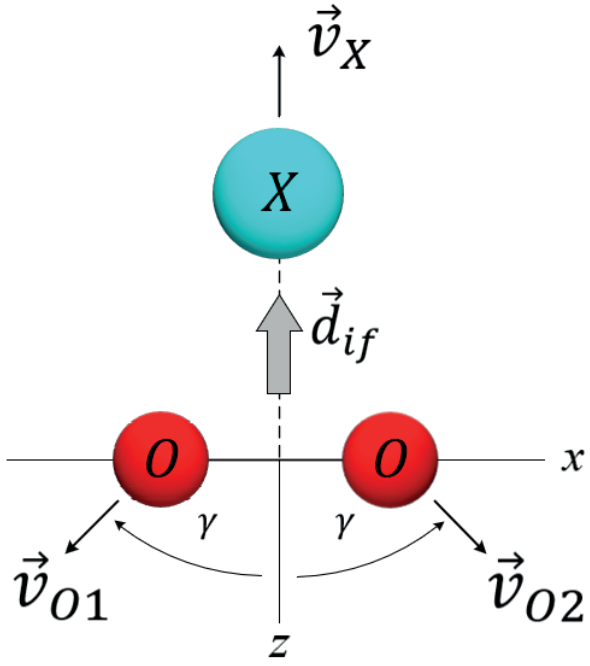


**Fig. 1.** The photodissociation scheme of the T-shaped complex X–$O_2$: $d_{if}$ – dipole moment of the excited transition ($i \rightarrow f$), γ – angle between the recoil direction of oxygen atoms and the symmetry axis of the complex.

the complex after simultaneous photoionization of both molecules in the complex by a powerful femtosecond laser pulse [7]. The results of this work confirm the dominance of the T-shaped complex structure, but provide a slightly larger value of the equilibrium distance Xe-$O_2$, equal to 4.07 Å. Earlier, Vidma et al. applied a new method for measuring the binding energy in van der Waals oxygen X-$O_2$ complexes based on the measurement of the velocity maps of oxygen atoms $O(^3P_j)$ arising in the X–$O_2$+$h\nu$→ X+O+O process [8]. In [8], the measurements for complexes with different X, including X=Xe, were carried out. For complex Xe-$O_2$ the van der Waals binding energy of 110 ± 20 $cm^{-1}$ was determined which is lower than the value obtained by Aquilanti et al. The difference in the data obtained in experiments with molecular beams may be due to the generation of complexes of different composition. In the present work, we have performed experiments in a wide range of conditions for van der Waals complexes generation, which allowed us to eliminate the contribution of other complexes to the results of measurements for Xe-$O_2$ complexes, as well as to provide the conditions for measuring the binding energy in more complicated $Xe_2$-$O_2$ complexes, which have not yet been studied.

## 2. VELOCITY MAP IMAGING TECHNIQUE AND ITS APPLICATION TO VAN DER WAALS BINDING ENERGY MEASUREMENT IN OXYGEN COMPLEXES

The velocity map imaging technique was used in this work. The technique was firstly implemented by Eppink and Parker [9], the main aspects of its application are described in the monograph [10]. The technique makes it possible to measure the distribution of photofragments in kinetic energy and in recoil directions with respect to the polarization of the excitation laser radiation. The measurements are realized in a molecular beam. The fragments formed as a result of photodissociation are further photoionized by laser radiation. Since the mass of electrons is very small, the distribution of velocities and directions of the flight of positively charged photoions coincides with the distribution for precursor neutral photo-fragments with good accuracy. A system of open electrodes is used to accelerate and focuse the photoions onto a two-dimensional detector that measures the arrival point of each ion. This focusing results in all ions of the same mass, having the same magnitude and direction of velocity, are focused to a single point on the detector, regardless of where the photoion is born. In this way, a two-dimensional projection of the 3-dimensional velocity distribution of photoions is measured. The 3-dimensional velocity distribution is reconstructed using the inverse Abel transform.

Earlier in the work by Vidma et al. it was shown that this technique can be used to measure the binding energy in the van der Waals complexes of oxygen with other molecules X-$O_2$ [8]. At the photon energy sufficient for photodissociation, the complex decays with the breaking of both the O-O

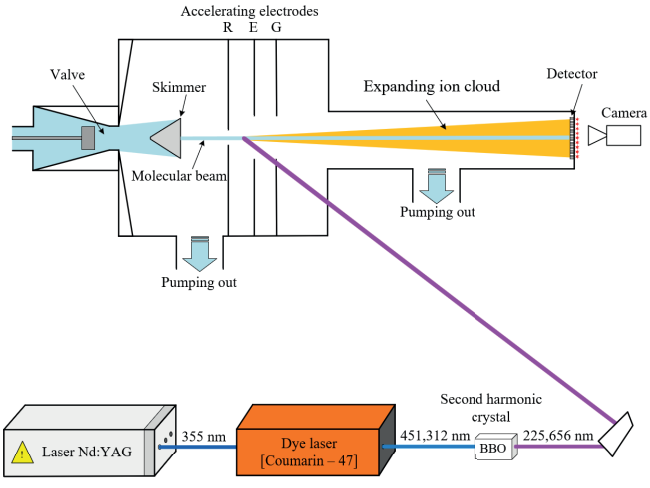


**Fig. 2**. The experimental setup.

bond and the van der Waals bond X-$O_2$ (in our experiments X=$Xe_n$)

$$X - O_2 \xrightarrow{h\nu} O(^3P_j) + O(^3P_j) + X. \quad (1)$$

Therefore, oxygen atoms from the complexes fly out with lower energy than in the photodissociation of unbound $O_2$ by radiation with the same wavelength. This difference in energy and angular anisotropy in the flight direction of the photofragments from the complex allows us to determine its binding energy.

Fig. 1 shows the kinematics of photofragment recoil upon excitation of T-shaped X-$O_2$ complexes. Excitation of X-$O_2$ complexes in the Hertzberg continuum region leads to the oxygen Hertzberg III state ($^3\Delta_u$) excitation [11]. This transition ($^3\Sigma_g^- \rightarrow {}^3\Delta_u$) is forbidden by orbital symmetry, but it becomes partially allowed in the complex due to the admixture of the charge transfer state of the complex [11,12]. As a consequence, the transition dipole moment is directed from the center of the oxygen molecule to the particle X, as shown in Fig. 1.

The distribution over the oxygen atoms recoil directions is described by the expression

$$I(\theta) = \frac{1 + \beta P_2(\cos\theta)}{4\pi}, \quad (2)$$

where $\beta = 3\cos^2\gamma - 1$ is the anisotropy parameter, $P_2(x) = (3x^2 - 1)/2$ is a Lejandre polynomial of the second degree, θ is the angle between the recoil direction and the polarization direction of the excitation laser radiation [8]. The angle γ is determined by the ratio of excess energy localized on the O-O bond and the X-$O_2$ bond in the excited state. Therewith, the anisotropy parameter $\beta \geqslant -1$, where the equality $\beta = -1$ takes place in the situation corresponding to the localization of total excitation on the O-O bond. The van der Waals energy of the X-$O_2$ bond can be derived from the measured values of the kinetic energy of oxygen atoms formed during free oxygen ($T_0$) and complexes ($T_1$) photodissociation, as well as the anisotropy parameter (β) for the oxygen atoms angular distribution over the recoil directions [8]

$$D(X - O_2) = 2T_0 - 2T_1\left(1 + \frac{2}{3}(1+\beta)\frac{m_O}{m_X}\right), \quad (3)$$

where $m_O / m_X$ is the atoms O and X mass ratio.

## 3. EXPERIMENTAL TECHNIQUE

The experimental setup described elsewhere [13] is shown in Fig. 2. A pulsed molecular beam (gas pulse duration of about 250 μs) was generated with an electrodynamic pulse valve, the design of which is described in [14], during supersonic expansion of gas into vacuum through a nozzle with a diameter of 500 μm.

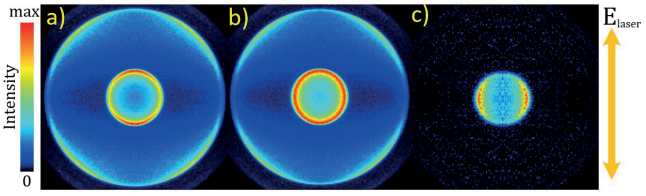


**Fig. 3**. Velocity maps of oxygen atoms formed during photodissociation: a)-oxygen molecules (composition of $O_2$ (1%)+He mixture, P=2 bar); b)-oxygen molecules and xenon complexes with oxygen ($O_2$ (1%)+Xe(1%)+He, P=2 bar); c)-xenon complexes with oxygen, the map was obtained by subtracting image (a) from image (b). The arrow on the right shows the direction of laser radiation polarization.

To generate $Xe_n$-$O_2$ and $Xe_n$ complexes, the valve was filled with a gas mixture of different composition: $O_2$ (from 0 to 7.5%) + Xe (from 0 to 4%) + He (balance) at a backing pressure varied from 1 to 4 bar. The central part of the beam formed by supersonic gas expansion into the vacuum chamber was extracted by a skimmer with a 2 mm hole located 6 cm from the nozzle so generated molecular beam entered the photoexcitation zone through an 8 mm diameter hole in the first electrode (repeller). The laser radiation was focused by a lens with a focal length of 17 cm onto molecular beam at a right angle. Laser radiation with a wavelength of 225.656 nm was used. It was obtained by doubling the radiation frequency of a pulsed dye laser (Coumarin-47) pumped by the 3rd harmonic of the Nd: YAG laser (LS-2137U, Lotis TII). The choice of such a wavelength is due to the fact that the energy of one photon of this radiation is sufficient for photodissociation of the oxygen molecule in a free state and in the complexes $Xe_n$-$O_2$. Moreover, at this wavelength the resonance-enhanced multiphoton ionization REMPI [2+1] of oxygen atoms in the ground $^3P_2$ state formed during photodissociation takes place. The formed ions are pulled by the electrodes into the free drift zone, where they fly away from the beam axis with velocities corresponding to those of the oxygen atoms formed by photodissociation. The open electrode system used focuses ions having the same magnitude and direction of velocity into a single point on the detector. A two-dimensional detector consisting of an assembly of F225–21P microchannel plates (Hamamatsu) captures the arrival point of each ion. To detect $O^+$ or $Xe^+$ photoions, the

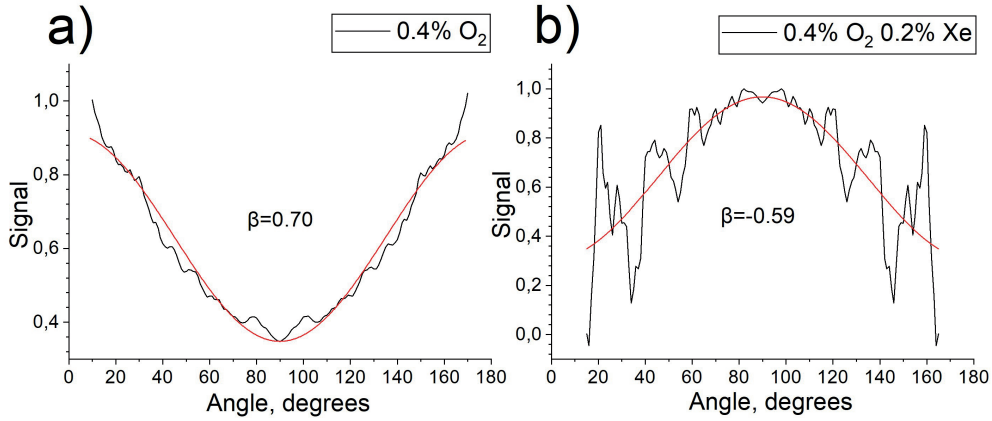


**Fig. 4.** Angular distribution over the recoil directions of oxygen atoms formed during photodissociation of an oxygen molecule (left) and xenon-oxygen complexes (right) with respect to the direction of excitation radiation polarization is shown. The values of the anisotropy parameter β obtained by fitting the angular distribution by expression (2) are shown in the figures.

detector is opened at the arrival time of the corresponding ions.

## 4. RESULTS

### 4.1 Oxygen atoms O($^3P_2$) velocity maps

Fig. 3 shows the obtained 2-dimensional images of oxygen atoms velocity maps, which we will hereafter call images. Fig. 3a shows the image of oxygen atoms formed by the photodissociation of unbound oxygen, Fig. 3b – by the photodissociation of the mixture of oxygen and xenon complexes with oxygen, and Fig. 3c is the result of subtracting image 3a from image 3b, which corresponds to the image of oxygen atoms formed from xenon-oxygen complexes. Images with similar shape were also observed at the other $O_2$ and Xe contents in the initial mixture. In Fig. 4 there are the results of the inversion of images of oxygen atoms O($^3P_2$) formed by single-photon excitation (inner ring in Fig. 3) of unbound oxygen and oxygen-xenon complexes. These results show the angular distribution over the directions of recoil with respect to the direction of polarization of the laser radiation, respectively. It is seen that the sign of the angular anisotropy parameter β changes for xenon-oxygen complexes.

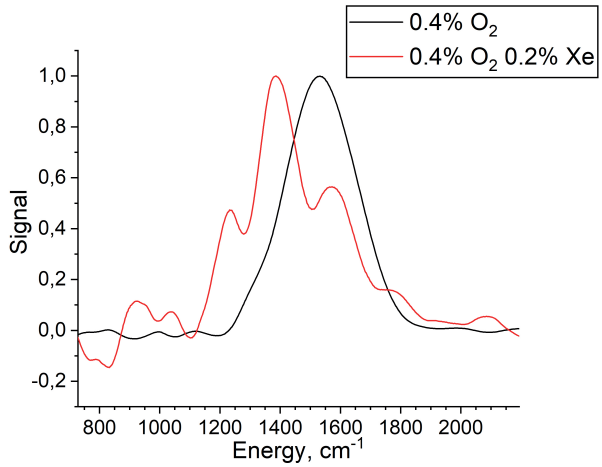


**Fig. 5**. Kinetic energy distribution for oxygen atoms O($^3P_2$) resulting from the photodissociation of unbound oxygen $O_2$ ($O_2$ (0.4%)+He, black line) and complexes xenon -oxygen ($O_2$ (0.4%)+Xe(0.2%)+He, red line), corresponding to the inner ring of images similar to those shown in Fig. 3p.

Fig. 5 shows the result of the image inversion for oxygen atoms arising from the single-photon photodissociation of unbound oxygen, as well as from xenon – oxygen complexes. It can be seen that the kinetic energy peak for oxygen atoms arising from photodissociation of the complexes shifts to lower energy values.

### 4.2 Velocity maps of xenon atoms

Fig. 6 shows images for $Xe^+$ photoions produced by focusing laser radiation $\lambda = 225.656$ nm , $h\nu = 5.494$ eV into a molecular beam formed by the expansion of $O_2$+Xe+He gas mixtures of different compositions.

All images show an intense signal of cold photoions in the center of the image, which arise from the non-resonant 3-photon ionization of free Xe atoms (ionization potential IP=12.13 eV [15]) in the beam. In addition, rings corresponding to photoions from xenon atoms with non-zero kinetic energy, which are formed by the decay of Xe complexes

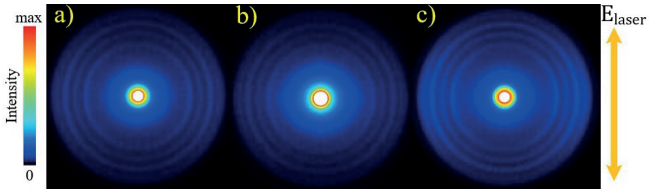


**Fig. 6**. Velocity maps of xenon atoms produced by focusing laser radiation (λ=225.656 nm) into the molecular beam formed by the expansion of gas mixtures (P=2 bar): a) $O_2$(1%)+Xe(1%)+He, b) Xe(1%)+He, and c) Xe(4%)+He. The contrast in case b) is increased for better visibility of the rings.

present in the gas mixture, are observed in all images. Since the observed rings are also present in the absence of oxygen (images 6b and 6c), it can be concluded that these are $Xe_n$ complexes. Fig. 7 shows the photoion velocity distribution obtained from the inversion of the images presented in Fig. 6.

## 5. DISCUSSIONS

### 5.1 Photodissociation of $O_2$

The velocity maps for oxygen atoms formed from photodissociation of the $O_2$ molecule by radiation of the Herzberg continuum spectral range were analyzed by Buijsse et al [18]. The image in Fig. 3a contains two rings. The inner ring corresponds to $O(^3P_2)$ atoms formed during the one-photon dissociation of $O_2$ molecule with the total kinetic energy of O atoms equal to 0.377 eV=3041 $cm^{-1}$, which corresponds to the difference between the photon energy hν=5.494 eV and the O-O bond breaking energy (5.117 eV, [18]). The bright outer ring corresponds to the dissociation of $O_2$ as a result of 2-photon excitation into the Schumann-Runge state with decay giving rise to a pair of $O(^3P)+O(^1D)$ atoms with total kinetic energy of 3.91 eV. The value of the angular anisotropy parameter for the inner ring measured in [18] was β=0.56. This value indicates the simultaneous contribution of two electrodipole transitions, parallel (Σ→Σ, β=2) and perpendicular (Σ→Π, β= −1). The outer ring has a quadrupole character of the angular dependence, which corresponds to the two-photon transitions Σ→Σ→Π and Σ→Π→Π, for which the angular dependence for the distribution over the recoil directions of oxygen atoms contains order 2 and 4 Lejandre polynomials [18].

$O(^3P_2)$ atoms velocity maps measurement for different oxygen contents in the initial gas mixture at a pressure of 2 bar showed that the inner ring diameter decreased with increasing $O_2$ content up to 2.5% and more. This decrease indicates the formation of larger size oxygen dimers and clusters, which consumes additional energy to break the van der Waals bonds. The formation of oxygen dimers, registered directly in the mass spectra of a molecular beam formed using a similar design valve and close in composition to the expanding gas mixture $O_2$(3%) + He (P=2 bar), was observed in [20]. To exclude the contribution of $O_2$-$O_2$ dimers, the oxygen concentration in our experiments with xenon complexes did not exceed 1% (full pressure in the valve 2 bar) and 0.4% (4 bar).

### 5.2 Photodissociation of Xe − $O_2$

Fig. 3c shows the image of $O(^3P_2)$ atoms arising from photodissociation of xenon-oxygen complexes. It is seen that the image has negative angular anisotropy. It is confirmed by the results of angular distribution processing presented in Fig. 4, which shows that the decay of oxygen-xenon complexes changes the sign of the anisotropy parameter β compared to the decay of free $O_2$. The results of the velocity map measuring for $O(^3P_2)$ formed from complexes generated at low xenon content (0.2 and 0.4%) in the initial gas mixture provide similar results, which we can ascribe to Xe-$O_2$ complexes. The negative anisotropy (β= −0.59 in Fig. 4b) for the decay of such complexes indicates their T-shaped

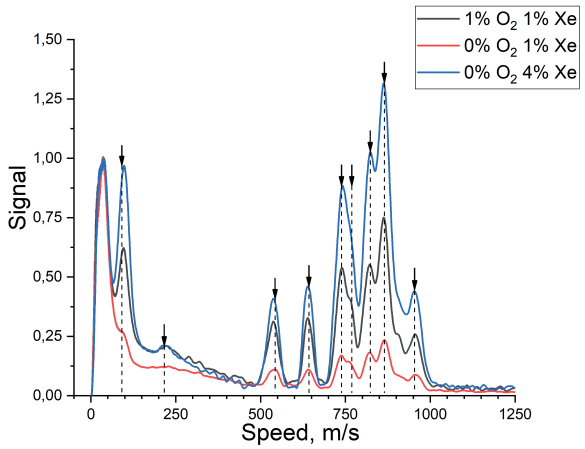


**Fig. 7**. Velocity distribution for $Xe^+$ photoions produced by focusing laser radiation (λ=225.656 nm, hν=5.494 eV) into the molecular beam formed by the expansion of $O_2$+Xe+He gas mixtures with oxygen and xenon contents indicated on the graph legend. The arrows show the velocity values of Xe atoms expected for the 2-photon dissociation of the xenon dimer $Xe_2$ decaying to form xenon atoms in Rydberg states (4), with the energy of the states given in the database [16]. To calculate the kinetic energy of the formed Xe atoms, the Xe-Xe bonding energy in the dimer was taken to be equal to the value of 197 $cm^{-1}$ given in [17].

structure. Figure 5 shows a decrease in the kinetic energy of $O(^3P_2)$ atoms compared to those formed during photodissociation of unbound oxygen. Averaging the results of measurements at low xenon content, taking into account the measurement error of the anisotropy parameter ($\Delta\beta=\pm0.1$) and using the expression (3), gives the value of the van der Waals binding energy in the T-shaped complex Xe-$O_2$ equal to $D(Xe\text{-}O_2) = 156\pm11$ cm$^{-1}$. The value of the binding energy measured by us using photofragment velocity maps agrees well with the result of Aquilanti et al 144±7 cm$^{-1}$ [6] obtained from the scattering of $O_2$ molecules on Xe atoms. The results obtained in this work also help to explain the reasons why a lower value was obtained in [8]. In paper [8], gas mixtures with higher (5%) oxygen content were used. As mentioned above in the discussion of the results on $O_2$ photodissociation, at higher $O_2$ contents (2.5% and higher), a noticeable contribution begins to be made by $O_2 - O_2$ dimers dissociation, whose decomposition produces oxygen atoms with lower kinetic energy than that from free $O_2$ molecules. Using the results of such a measurement as a reference value corresponding to the decomposition of unbound $O_2$ lead to the underestimation of the determined binding energy in X-$O_2$ complexes.

### 5.3 Photodissociation of $Xe_2 - O_2$

It was observed, that further xenon content increase in the gas mixture (up to 1–2%) leads to the oxygen atoms kinetic energy shift to lower values $T_1$=1339–1355 cm$^{-1}$, which corresponds to the photodissociation of oxygen complexes with a larger xenon atoms number. It can be assumed that during the expansion of the gas mixture with an increased xenon content, xenon dimers $Xe_2$ are formed as the simplest clusters, which further recombine with oxygen to form the complex $Xe_2$-$O_2$.

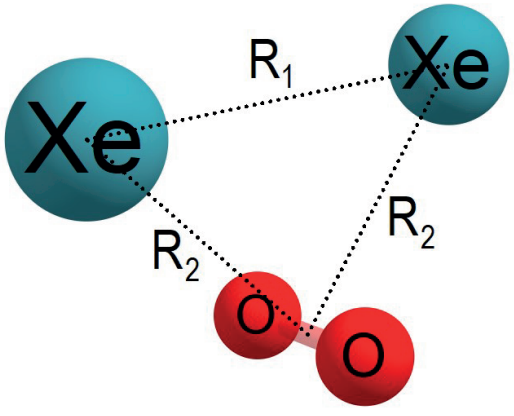


**Fig. 8**. $Xe_2$-$O_2$ complex structure (see the text).

The dimer formation under these conditions is confirmed by the observed $Xe^+$ photoion velocity maps, the inversion results of which are shown in Fig. 7. The position of the $Xe^+$ photoion peaks observed in the figure corresponds well to the velocity values expected for the atoms formed by the 2-photon dissociation of a xenon dimer $Xe_2$, which decays to xenon atoms in Rydberg states Xe(Ry) with energies given in the database [16]. The formation of Rydberg atoms Xe(Ry) is provided by their one-photon ionization:

$$Xe_2 + 2h\nu \rightarrow Xe + Xe(Ry), \quad (4)$$

$$Xe(Ry) + h\nu \rightarrow Xe^+ + e. \quad (5)$$

The oxygen atom in the photodissociation of the $Xe_2$-$O_2$ complex is formed in the process of

$$Xe_2 - O_2 + h\nu \rightarrow O + O + Xe_2. \quad (6)$$

The image of oxygen atoms formed under conditions corresponding to the formation of $Xe_2$-$O_2$ complexes (see Fig. 3c) is also characterized by a negative value of the anisotropy parameter (the measured β lie in the range from –0.60 to –0.73), indicating that the $Xe_2$-$O_2$ complex is also T-shaped, i.e., the center of the $Xe_2$ fragment is located perpendicular to the $O_2$ axis. The structure of this complex can be constructed taking into account that the van der Waals interaction of Xe atoms with each other and of each Xe atom with the $O_2$ molecule should be considered independently. The most stable configuration with the T-shaped orientation of each Xe atom with respect to $O_2$ is the structure shown in Fig. 8. Accordingly, to calculate the van der Waals binding energy of $Xe_2$-$O_2$ using expression (3), the mass is equated to twice the mass of a Xe atom. Averaging the measurement results at higher xenon content (1 and 2%), and taking into account the measurement error of the anisotropy parameter ($\Delta\beta=\pm0.1$), we obtain the value of the binding energy $D(Xe_2\text{-}O_2) = 314\pm30$ cm$^{-1}$. For the structure shown in Fig. 8, this binding energy should be close to twice the value of the binding energy D(Xe-$O_2$), which is consistent with the results of our measurements. The O+O+Xe bond length in the complex in Fig. 8 can be assumed to be $R_1$=4.37 Å for this distance in the $Xe_2$ dimer determined in [17]. The distance $R_2$ in Fig. 8 should be considered close to the value of 3.87 Å determined by Aquilanti et al. in [6] for the Xe-$O_2$ complex.

## 6. CONCLUSION

In this work, the van der Waals binding energy in xenon-oxygen complexes is measured using the photofragment

velocity map imaging technique. The velocity maps allow us to measure the photofragments distribution over their kinetic energy and recoil directions with respect to the polarization direction of the excitation radiation. The generation of xenon-oxygen complexes took place in a cold supersonic molecular beam. The complexes excitation and subsequent resonance-enhanced multiphoton ionization by REMPI (2+1) of the arising oxygen atoms were performed using tunable laser radiation.

To determine the van der Waals binding energy of oxygen in the complexes, the velocity maps of oxygen atoms formed from unbound oxygen molecules and from $O_2$ molecules in complex with xenon atoms were measured. It is shown that the sign of the angular anisotropy parameter changes in case of the photodissociation of xenon-bounded $O_2$ molecule, which indicates the T-shaped structure of xenon-oxygen complexes in which the $O_2$ molecule is oriented perpendicular to the direction of oxygen-xenon binding. The results of the velocity maps measuring at low xenon concentration in the expanding mixture allowed us to measure the van der Waals binding energy in Xe-$O_2$ complexes equal to $D(Xe\text{-}O_2) = 156\pm11$ cm$^{-1}$. With increasing xenon content in the initial gas mixture, photogeneration of oxygen atoms with lower kinetic energy was registered. It was ascribed to the appearance of complexes containing two xenon atoms $Xe_2$-$O_2$. This attribution is confirmed by the simultaneous appearance of xenon dimers $Xe_2$, which was recorded by the appearance of translationally "hot" xenon atoms. Measured kinetic energy of such "hot" atoms corresponds exactly to that expected for the dimers photodissociation. The results of the velocity maps measurement of oxygen atoms formed from $Xe_2$-$O_2$ complexes allowed us to determine the van der Waals binding energy of oxygen in these complexes, equal to $D(Xe_2\text{-}O_2) = 314\pm30$ cm$^{-1}$. The results obtained allowed us to propose the structure of $Xe_2$-$O_2$ complexes. Also, the results obtained in this work confirm the power of the photofragment velocity map technique in measuring the binding energy in van der Waals complexes of oxygen.

## REFERENCES


1. S.C. Cullen, E.G. Gross, The anesthetic properties of xenon in animals and human beings, with additional observations on krypton, Science, 113, p. 580–582 (1951).
2. T.L. Liu, Y. Xu, P. Tang, J. Phys. Chem. B, 114, p. 9010–9016 (2010).
3. N.N. Andrijchenko, A. Yu. Ermilov, L. Khriachtchev et al., The Journal of Physical Chemistry A, 119, p. 2517–2521 (2015).
4. N. Li., D. Lu, L. Yang et al., Anesthesiology, 129, p. 271–277 (2018).
5. J. Smith, H.Z. Haghighi, D. Salahub et al., Sci. Rep., 11, 6287 (2021).
6. V. Aquilanti, D. Ascenzi, D. Cappelletti et al., J. Chem. Phys., 109, 3898 (1998).
7. J. Wu, M. Kunitski, L. Ph.H. Schmidt et al., J. Chem. Phys., 137, 104308 (2012).
8. K.V. Vidma, G.A. Bogdanchikov, A.V. Baklanov et al., J. Chem. Phys., 133, 194306 (2010).
9. A.T.J.B. Eppink, D.H. Parker, Rev. Sci. Instrum., 68, 3477 (1997).
10. Imaging in molecular dynamics. Technology and applications. Ed. B.J. Whitaker, Cambridge, University Press (2003).
11. A.V. Baklanov, G.A. Bogdanchikov, K.V. Vidma et al., J. Chem. Phys., 126, 124316 (2007).
12. A.V. Baklanov, D. Parker, Kinetics and Catalysis, 61, pp. 168–194 (2020).
13. A.S. Bogomolov, V.G. Goldort, S.A. Kochubei et al., J. Chem. Phys., 147, 234304 (2017).
14. V.N. Ishchenko, S.A. Kochubei, V.I. Makarov et al., On cooling of vibrationally excited benzene molecules in supersonic molecular beams, Chem. Phys. Lett., 299, p. 227–232 (1999).
15. Ionization potentials of atoms and atomic ions, ed. by D.R. Lide, Handbook of Chem. and Phys., p. 10–211 (1992).
16. A. Kramida, Yu. Ralchenko, J. Reader et al., NIST Atomic Spectra Database (version 5.10), National Institute of Standards and Technology, Gaithersburg, MD (2022).
17. A.K. Dham, W.J. Meath, A.R. Allnatt et al., XC and HFD-B potential energycurves for Xe-Xe and related physical properties, Chemical Physics, 142, p. 173–189 (1990).
18. B. Buijsse, W.J. van der Zande, A.T.J.B. Eppink et al., J. Chem. Phys., 108, 7229 (1998).
19. P.C. Cosby, D.L. Huestis, J. Chem. Phys., 97, 6108 (1992).
20. A.E. Zarvin, N.G. Korobeishchikov, V.V. Kalyada et al., Eur. Phys. J. D, 49, p. 101–110 (2008).